


Designing effective thermal conductivity of materials of core-shell structure: Theory and simulation

LiuJun Xu, Shuai Yang, and Jiping Huang*

Department of Physics, State Key Laboratory of Surface Physics, and Key Laboratory of Micro and Nano Photonic Structures (MOE), Fudan University, Shanghai 200433, China

 (Received 2 November 2018; published 7 February 2019)

We introduce the phenomenon of golden touch from myth to thermotics. We define golden touch as extending the core property to a shell with an extremely small core fraction. We obtain the requirement of golden touch by making the effective thermal conductivity of the core-shell structure equal to the thermal conductivity of the core. We summarize three types (A, B, and C) of golden touch in two dimensions, and only two types (A and B) of golden touch in three dimensions. We theoretically analyze the distinct properties of different types of golden touch by delicately designing the anisotropic thermal conductivity of the shell. Golden touch is also validated by finite-element simulations which echo the theoretical analyses. Golden touch has potential applications in thermal camouflage, thermal management, etc. Our work not only lays the foundation for golden touch in thermotics, but also provides guidance for exploring golden touch in other diffusive fields like electrostatic and magnetostatic fields.

DOI: [10.1103/PhysRevE.99.022107](https://doi.org/10.1103/PhysRevE.99.022107)

I. INTRODUCTION

Golden touch is a long-standing dream of human beings which exists only in myth. To uncover the secret of golden touch, we should first define what golden touch is. We refer to the core-shell structure as our research object; see the middle structure in Fig. 1. For simplicity of understanding, we may imagine the shell as “stone” and the core as “gold.” Then golden touch can be defined as extending the core property to the shell with zero core fraction, i.e., an imaginary core. Such a definition is what the golden touch in myth describes.

In spite of the difficulty, we do not give up the exploration of golden touch. Although we cannot extend the core property to the shell with zero core fraction, we may resort to some loosened requirements which are physical. Hence, here we define golden touch as extending the core property to the shell with extremely small core fraction. We only replace the requirement of zero core fraction with extremely small core fraction. The redefinition of golden touch does not affect the inconceivable phenomenon and makes possible realization. Concretely speaking, a normal case presents only a slow increment with core fraction; see the black (lower right) line in Fig. 1. In other words, if the effective core-shell property is expected to exhibit the core property, the core fraction should be 1, which echoes with the common sense of effective medium theories [1–4]. By contrast, golden touch presents a steep increment with core fraction; see the red (upper left) line in Fig. 1. In other words, “stone” can become “gold” with an extremely small “gold” fraction. This is what we expect to obtain.

In this work, we focus on the thermal property of the core-shell structure, i.e., effective thermal conductivity. In fact,

research on artificial structures has realized many unique phenomena, such as thermal cloaks [5–10], thermal concentrators [6,11–14], thermal camouflage [15–21], etc. Differently from these, we carefully design the anisotropic shell to realize golden touch, especially when the thermal conductivity of the shell is abnormal ($\kappa_{\theta\theta}/\kappa_{rr} < 0$ for two dimensions and $\kappa_{\theta\theta}/\kappa_{rr} < -1/8$ for three dimensions). The potential application of golden touch is to dramatically reduce the use of special materials (only with extremely small core fraction). Moreover, golden touch may also provide guidance for thermal camouflage, such as size misleading.

II. THEORY OF GOLDEN TOUCH

We first discuss the golden touch in two-dimensional core-shell structure; see Fig. 2(a). We set the core with radius r_c and scalar thermal conductivity κ_c , and the shell with radius r_s and tensorial thermal conductivity $\kappa_s = \text{diag}(\kappa_{rr}, \kappa_{\theta\theta})$. We can derive the effective thermal conductivity of the core-shell structure κ_e as

$$\kappa_e(\kappa_{\theta\theta}/\kappa_{rr} > 0) = m\kappa_{rr} \frac{\kappa_c + m\kappa_{rr} + (\kappa_c - m\kappa_{rr})(\sqrt{p})^{2m}}{\kappa_c + m\kappa_{rr} - (\kappa_c - m\kappa_{rr})(\sqrt{p})^{2m}}, \quad (1)$$

$$\kappa_e(\kappa_{\theta\theta}/\kappa_{rr} < 0) = n\kappa_{rr} \frac{\kappa_c + n\kappa_{rr} \tan(n \ln \sqrt{p})}{n\kappa_{rr} - \kappa_c \tan(n \ln \sqrt{p})}, \quad (2)$$

where $m = \sqrt{\kappa_{\theta\theta}/\kappa_{rr}}$, $n = \sqrt{-\kappa_{\theta\theta}/\kappa_{rr}}$, and $p = (r_c/r_s)^2$ is the core fraction. A detailed derivation can be found in the Appendix.

We calculate the limit of Eqs. (1) and (2) to discuss the property when $\kappa_{\theta\theta}/\kappa_{rr} = 0$ and find that they tend to the

*jphuang@fudan.edu.cn

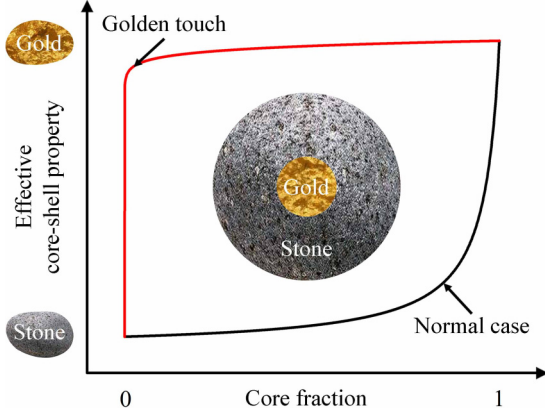


FIG. 1. Schematic diagram of golden touch (vs normal case). “Gold” and “stone” are metaphors for simplicity of understanding.

same value

$$\kappa_e(\kappa_{\theta\theta}/\kappa_{rr} = 0) = \kappa_{rr} \frac{\kappa_c - \kappa_{\theta\theta} \ln \sqrt{p}}{\kappa_{rr} - \kappa_c \ln \sqrt{p}}. \quad (3)$$

Note that κ_e is still dependent on $\kappa_{\theta\theta}$ despite $\kappa_{\theta\theta}/\kappa_{rr} = 0$, because there is a condition of $\kappa_{rr} \gg \kappa_{\theta\theta} (\neq 0)$ to satisfy $\kappa_{\theta\theta}/\kappa_{rr} = 0$. Moreover, $\kappa_{\theta\theta}/\kappa_{rr} = 0$ can be regarded as the demarcation point according to Eqs. (1)–(3).

As the definition suggests, golden touch should first ensure that the core property can be extended to the shell, which can be mathematically expressed as

$$\kappa_e = \kappa_c. \quad (4)$$

Notice that $\kappa_e(p=0) \neq \kappa_c$, otherwise the shell is just the same as the core, which is trivial.

Second, golden touch should ensure the extremely small core fraction, which can be mathematically expressed as

$$p = 0^+. \quad (5)$$

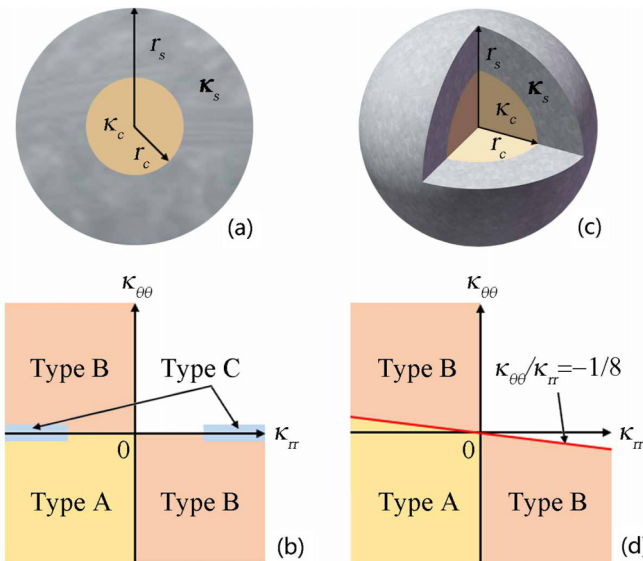


FIG. 2. Golden touch in (a, b) two dimensions and (c, d) three dimensions. Panels (a, c) and (b, d), respectively, present the structures and classifications of golden touch.

Equations (4) and (5) can be regarded as the mathematical definition of golden touch.

After investigating Eqs. (1)–(3), we find three types (A, B, and C) of golden touch in two dimensions which satisfy the requirements of Eqs. (4) and (5):

$$\text{Type A} \rightarrow \kappa_{\theta\theta}/\kappa_{rr} > 0: \kappa_c + m\kappa_{rr} = 0, \quad (6)$$

$$\text{Type B} \rightarrow \kappa_{\theta\theta}/\kappa_{rr} < 0: \sqrt{-\kappa_{\theta\theta}/\kappa_{rr}} \ln \sqrt{p} = -Z^+ \pi, \quad (7)$$

$$\text{Type C} \rightarrow \kappa_{\theta\theta}/\kappa_{rr} \approx 0: \kappa_{\theta\theta} \approx 0 \text{ with } \kappa_{rr} \gg \kappa_1, \quad (8)$$

where $Z^+ (= 1, 2, 3, \dots)$ is positive integers. The three types (A, B, and C) of golden touch are clearly presented in Fig. 2(b), which respectively correspond to the $>$, $<$, and \approx demarcation point.

We then discuss the golden touch in a three-dimensional core-shell structure; see Fig. 2(c). We set the core with radius r_c and scalar thermal conductivity κ_c , and the shell with radius r_s and tensorial thermal conductivity $\kappa_s = \text{diag}(\kappa_{rr}, \kappa_{\theta\theta}, \kappa_{\phi\phi})$ with $\kappa_{\theta\theta} = \kappa_{\phi\phi}$ for brevity. We can derive the effective thermal conductivity of the core-shell structure κ_e as

$$\begin{aligned} \kappa_e(\kappa_{\theta\theta}/\kappa_{rr} > -1/8) &= \kappa_{rr} \frac{u_1(\kappa_c - u_2\kappa_{rr}) - u_2(\kappa_c - u_1\kappa_{rr})(\sqrt[3]{p})^{u_1 - u_2}}{(\kappa_c - u_2\kappa_{rr}) - (\kappa_c - u_1\kappa_{rr})(\sqrt[3]{p})^{u_1 - u_2}}, \end{aligned} \quad (9)$$

$$\begin{aligned} \kappa_e(\kappa_{\theta\theta}/\kappa_{rr} < -1/8) &= \kappa_{rr} \frac{4v\kappa_c + [2\kappa_c + (1 + 4v^2)\kappa_{rr}] \tan(v \ln \sqrt[3]{p})}{4v\kappa_{rr} - 2(2\kappa_c + \kappa_{rr}) \tan(v \ln \sqrt[3]{p})}, \end{aligned} \quad (10)$$

where $u_{1,2} = (-1 \pm \sqrt{1 + 8\kappa_{\theta\theta}/\kappa_{rr}})/2$, $v = \sqrt{-1 - 8\kappa_{\theta\theta}/\kappa_{rr}}/2$, and $p = (r_c/r_s)^3$ is the core fraction. Detailed derivation can be found in the Appendix.

We calculate the limit of Eqs. (9) and (10) to discuss the property when $\kappa_{\theta\theta}/\kappa_{rr} = -1/8$, and find that they tend to the same value:

$$\kappa_e(\kappa_{\theta\theta}/\kappa_{rr} = -1/8) = \kappa_{rr} \frac{4\kappa_c + (2\kappa_c + \kappa_{rr}) \ln \sqrt[3]{p}}{4\kappa_{rr} - 2(2\kappa_c + \kappa_{rr}) \ln \sqrt[3]{p}}. \quad (11)$$

Here $\kappa_{\theta\theta}/\kappa_{rr} = -1/8$ can be regarded as the demarcation point according to Eqs. (9)–(11).

We also calculate the effective thermal conductivity when $\kappa_{\theta\theta}/\kappa_{rr} = 0$ as a special case:

$$\kappa_e(\kappa_{\theta\theta}/\kappa_{rr} = 0) = \kappa_{rr} \frac{\kappa_c \sqrt[3]{p}}{\kappa_{rr} + \kappa_c(1 - \sqrt[3]{p})}. \quad (12)$$

Here κ_e is independent of $\kappa_{\theta\theta}$ which is different from the two-dimensional result of Eq. (3).

According to the mathematical definition of golden touch Eqs. (4) and (5), we investigate Eqs. (9)–(12) but find only two types (A and B) of golden touch:

$$\text{Type A} \rightarrow \kappa_{\theta\theta}/\kappa_{rr} > -1/8: \kappa_c - u_2\kappa_{rr} = 0, \quad (13)$$

$$\begin{aligned} \text{Type B} \rightarrow \kappa_{\theta\theta}/\kappa_{rr} < -1/8: (\sqrt{-1 - 8\kappa_{\theta\theta}/\kappa_{rr}}/2) \ln \sqrt[3]{p} &= -Z^+ \pi, \end{aligned} \quad (14)$$

where $Z^+ (= 1, 2, 3, \dots)$ is positive integers. The two types (A and B) of golden touch are clearly presented in Fig. 2(d),

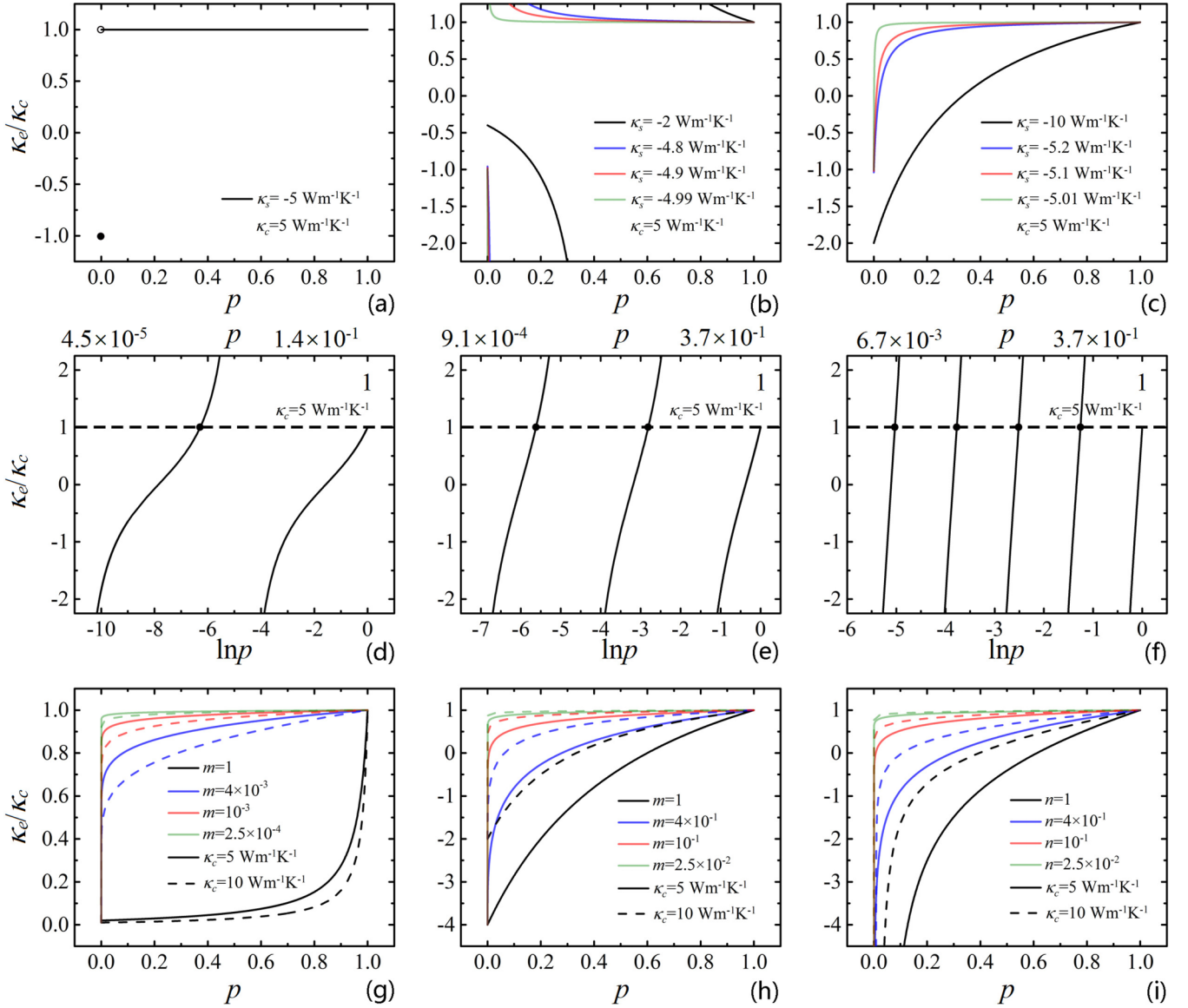


FIG. 3. Theoretical analyses of two-dimensional golden touch for (a–c) type A, (d–f) type B, and (g–i) type C. Concrete parameters: (a–c) $\kappa_c = 5 \text{ Wm}^{-1} \text{ K}^{-1}$, and the thermal conductivity of the shell is a scalar denoted as κ_s ; (d–f) $\kappa_c = 5 \text{ Wm}^{-1} \text{ K}^{-1}$, $\kappa_{rr} = 5 \text{ Wm}^{-1} \text{ K}^{-1}$, (d) $n = 1$, (e) $n = \sqrt{5}$, and (f) $n = 5$; (g–i) $\kappa_c = 5 \text{ Wm}^{-1} \text{ K}^{-1}$ for solid lines, $\kappa_c = 10 \text{ Wm}^{-1} \text{ K}^{-1}$ for dashed lines, (g) $m\kappa_{rr} = 0.1 \text{ Wm}^{-1} \text{ K}^{-1}$, (h) $m\kappa_{rr} = -20 \text{ Wm}^{-1} \text{ K}^{-1}$, and (i) $n\kappa_{rr} = 20 \text{ Wm}^{-1} \text{ K}^{-1}$. It should be noted that there are three lines in the left bottom of (b), which are very close to each other.

which respectively correspond to the $>$ and $<$ demarcation point. Differently from a two-dimensional system, there is no type C golden touch in a three-dimensional system, even though we carefully calculate the effective thermal conductivity of the core-shell structure when $\kappa_{\theta\theta}/\kappa_{rr} = -1/8$ [demarcation point in three dimensions; Eq. (11)], or $\kappa_{\theta\theta}/\kappa_{rr} = 0$ [Eq. (12)].

III. THEORETICAL ANALYSES OF GOLDEN TOUCH

We further analyze the distinct properties of different types of golden touch. For clarity, we discuss the dimensionless thermal conductivity κ_e/κ_c . When $\kappa_e/\kappa_c = 1$, the core property is extended to the shell.

The two-dimensional results of type A, type B, and type C golden touch are, respectively, demonstrated in Figs. 3(a)–3(c), 3(d)–3(f), and 3(g)–3(i). We will give detailed discussions of the three types of golden touch in the following.

Type A: When the requirement of Eq. (6) is strictly satisfied, there is a discontinuous change from -1 to 1 at $p = 0$; see Fig. 3(a). In other words, the core property can be extended to the shell with arbitrarily small core fraction once $p \neq 0$. We increase the thermal conductivity of the shell [see Fig. 3(b)], and the variation curves become similar to a hyperbolic function. When the increment is small enough, golden touch still works; see the green (lightest) line in Fig. 3(b). However, when the increment is big, golden touch turns into the normal case; see the black (darkest) line in Fig. 3(b). We decrease the thermal conductivity of the shell [see Fig. 3(c)],

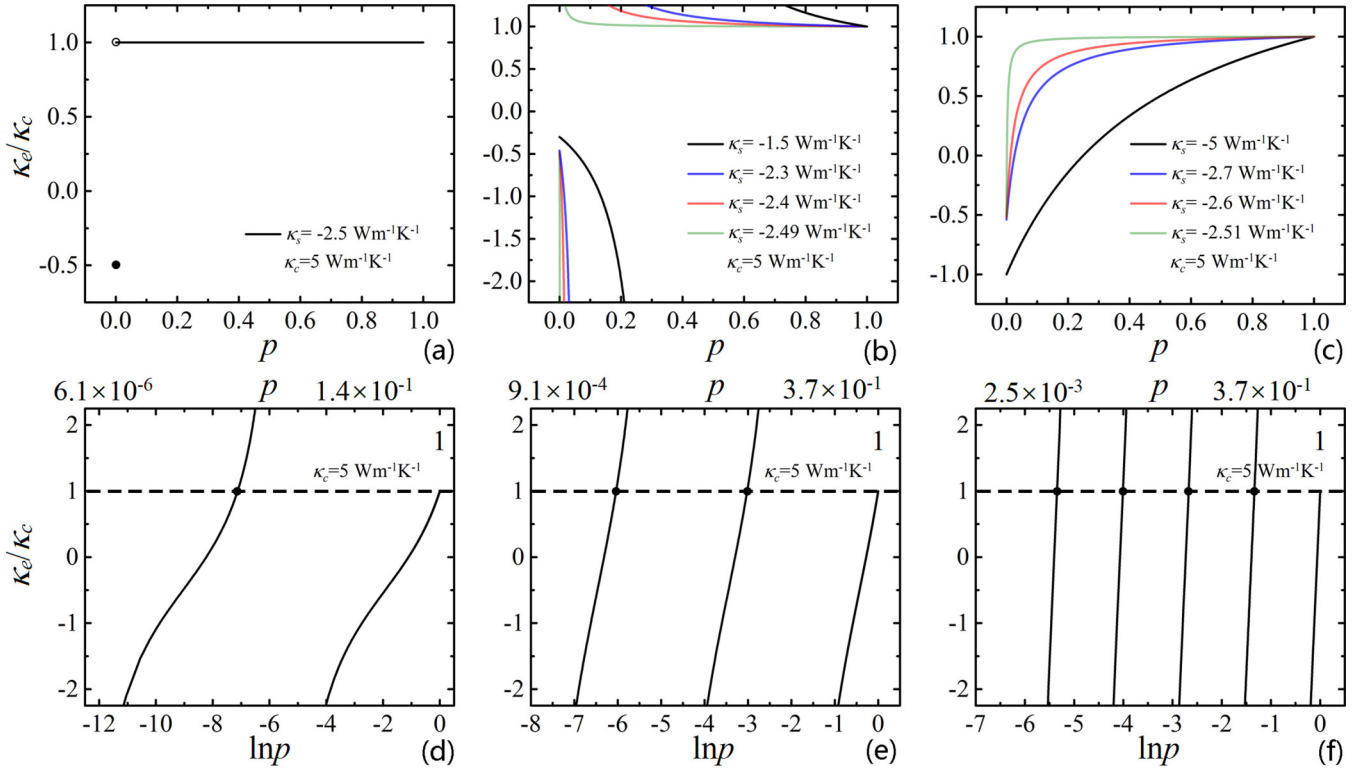


FIG. 4. Theoretical analyses of three-dimensional golden touch for (a–c) type A and (d–f) type B. Concrete parameters: (a–c) $\kappa_c = 5 \text{ Wm}^{-1}\text{K}^{-1}$, and the thermal conductivity of the shell is a scalar denoted as κ_s ; (d–f) $\kappa_c = 5 \text{ Wm}^{-1}\text{K}^{-1}$, $\kappa_{rr} = 5 \text{ Wm}^{-1}\text{K}^{-1}$, (d) $v = \sqrt{7}/2$, (e) $v = \sqrt{39}/2$, and (f) $n = \sqrt{199}/2$.

and the variation curves become monotonically increasing without a discontinuous change. When the decrement is small enough, golden touch still works; see the green (lightest) line in Fig. 3(c). However, when the decrement is big, golden touch turns into the normal case; see the black (darkest) line in Fig. 3(c). Therefore, type A golden touch can work perfectly with arbitrarily small core fraction, but requires a special relation of thermal conductivities between the core and the shell.

Type B: In fact, as long as $\kappa_{\theta\theta}/\kappa_{rr} < 0$, the phenomena of golden touch will exist, for the curve value ranges from $-\infty$ to $+\infty$ and presents quasiperiodicity; see Figs. 3(d)–3(f). The quasiperiodicity is determined by the shell anisotropy: from left to right of Figs. 3(d)–3(f), the smaller $\kappa_{\theta\theta}/\kappa_{rr}$ is (or the bigger n is), the denser quasiperiodicity is. Therefore, type B golden touch can work perfectly without requirement of thermal conductivities between the core and the shell, but with a certain core fraction determined by Eq. (7); see the dots in Figs. 3(d)–3(f). Note that we use $\ln p$ (ranging from $-\infty$ to 0) as the abscissa to show the infinite numbers of quasiperiodicity, and hence the core fraction can also be set as arbitrarily small.

Type C: The parameters of Eq. (8) are distributed in four quadrants; see Fig. 2(b). When $\kappa_{\theta\theta}/\kappa_{rr}$ is in the third quadrant, type C golden touch possesses all the properties of type A golden touch. When $\kappa_{\theta\theta}/\kappa_{rr}$ is in the second (or fourth) quadrant, type C golden touch possesses all the properties of type B golden touch. Even so, we still regard type C golden touch as a separate classification, for it possesses different properties from type A and type B golden touch. Concretely

speaking, type A and type B golden touch require certain thermal conductivity [Eq. (6)] or core fraction [Eq. (7)], but these requirements disappear in type C golden touch. In other words, any thermal conductivity can be extended with any core fraction. The costs are (I) the requirement of Eq. (8), and (II) the core fraction can be only extremely small rather than arbitrarily small, which is dependent on the shell. We take the parameters in the first quadrant as an example; see Fig. 3(g). Solid and dashed lines, respectively, correspond to the different thermal conductivities of cores. With the decrement of $m (= \sqrt{\kappa_{\theta\theta}/\kappa_{rr}} \rightarrow 0)$, the core property can be extended to shell regardless of the core conductivities; see the green (lightest) solid and dashed lines in Fig. 3(g). We also investigate parameters in the third and fourth quadrants, and the results are, respectively, shown in Figs. 3(h) and 3(i) which are similar to those in Fig. 3(g). Note that the reason why the variation curves in Fig. 3(i) do not present the quasiperiodicity with $\kappa_{\theta\theta}/\kappa_{rr} < 0$ is that the quasiperiodicity becomes sparse with small n (as discussed in type B golden touch), and thus exists in extremely small core fraction, which cannot be shown under the abscissa of p .

The three-dimensional results of type A and type B golden touch are, respectively, demonstrated in Figs. 4(a)–4(c) and 4(d)–4(f). Except for that there is no type C golden touch in three dimensions, type A and type B golden touch in three dimensions are similar to those in two dimensions.

Type A: When the requirement of Eq. (13) is strictly satisfied, there is a discontinuous change from -0.5 to 1 at $p = 0$; see Fig. 4(a). We increase the thermal conductivity of the shell [see Fig. 4(b)], and the variation curves become

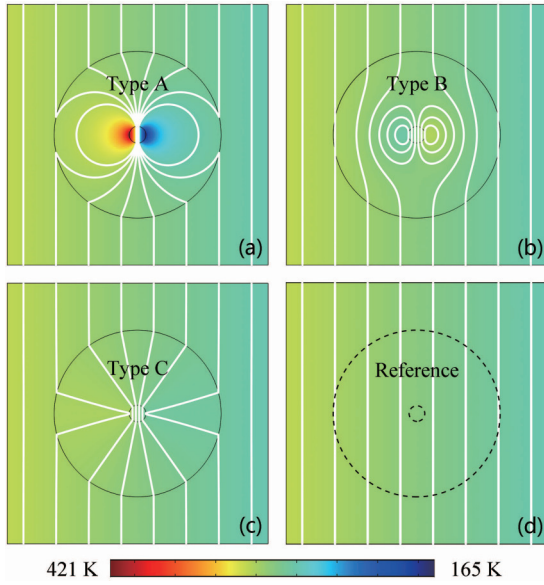


FIG. 5. Finite-element simulations of two-dimensional golden touch for (a) type A, (b) type B, (c) type C, and (d) reference. Concrete parameters: (a–d) simulation box is 20×20 cm, $r_s = 6.4$ cm, $r_c = 0.64$ cm, $\kappa_c = \kappa_m = 5 \text{ Wm}^{-1}\text{K}^{-1}$, (a) $\kappa_s = -5.001 \text{ Wm}^{-1}\text{K}^{-1}$, (b) $\kappa_s = \text{diag}(5, -9.308) \text{ Wm}^{-1}\text{K}^{-1}$, (c) $\kappa_s = \text{diag}(400, 2.5 \times 10^{-6}) \text{ Wm}^{-1}\text{K}^{-1}$, and (d) $\kappa_s = 5 \text{ Wm}^{-1}\text{K}^{-1}$. Dashed lines in panel (d) are used to show the imaginary location of the core-shell structure for simplicity of comparison. The left and right boundaries are, respectively, set at 313 K and 273 K, and other boundaries are insulated. White lines represent isotherms.

similar to a hyperbolic function. When the increment is small enough, golden touch still works; see the green (lightest) line in Fig. 4(b). However, when the increment is big, golden touch turns into the normal case; see the black (darkest) line in Fig. 4(b). We decrease the thermal conductivity of the shell [see Fig. 4(c)], and the variation curves become monotonically increasing without a discontinuous change. When the decrement is small enough, golden touch still works; see the green (lightest) line in Fig. 4(c). However, when the decrement is

big, golden touch turns into the normal case; see the black (darkest) line in Fig. 4(c). Therefore, type A golden touch can work perfectly with arbitrarily small core fraction, but requires a special relation of thermal conductivities between the core and the shell.

Type B: As long as $\kappa_{\theta\theta}/\kappa_{rr} < -1/8$, the phenomenon of golden touch will exist, for the curve value ranges from $-\infty$ to $+\infty$ and present quasiperiodicity; see Figs. 4(d)–4(f). The quasiperiodicity is determined by the shell anisotropy: from left to right in Figs. 4(d)–4(f), the smaller $\kappa_{\theta\theta}/\kappa_{rr}$ is (or the bigger v is), the denser quasiperiodicity is. Therefore, type B golden touch can work perfectly without the requirement of thermal conductivities between the core and the shell, but with certain core fraction determined by Eq. (14); see the dots in Figs. 4(d)–4(f). We also use $\ln p$ (ranging from $-\infty$ to 0) as the abscissa to show the infinite numbers of quasiperiodicity, and hence the core fraction can also be set as arbitrarily small.

IV. FINITE-ELEMENT SIMULATIONS OF GOLDEN TOUCH

We have theoretically analyzed the distinct properties of different types of golden touch in both two and three dimensions. Now we are in the position to demonstrate finite-element simulations for an intuitive understanding of golden touch. We put the core-shell structure into a matrix (κ_m) with the same thermal conductivity of the core ($\kappa_m = \kappa_c$). If golden touch does extend the core property to shell, the external thermal field will keep unchanged, namely, uniform temperature gradient. To be mentioned, although the core fraction of type A and type B golden touch can be arbitrarily small, we have to set the core fraction as a reasonable finite small value to perform finite-element simulations based on the commercial software COMSOL Multiphysics [22].

The results of two-dimensional golden touch are presented in Fig. 5. We set the core fraction as 0.01. Type A, type B, and type C golden touch are, respectively, designed according to Eqs. (6)–(8). For type C golden touch, this is not an exact result (extremely small rather than arbitrarily small), for the parameters applied for finite-element simulation echo the green (lightest) solid line in Fig. 3(g). The same uniform

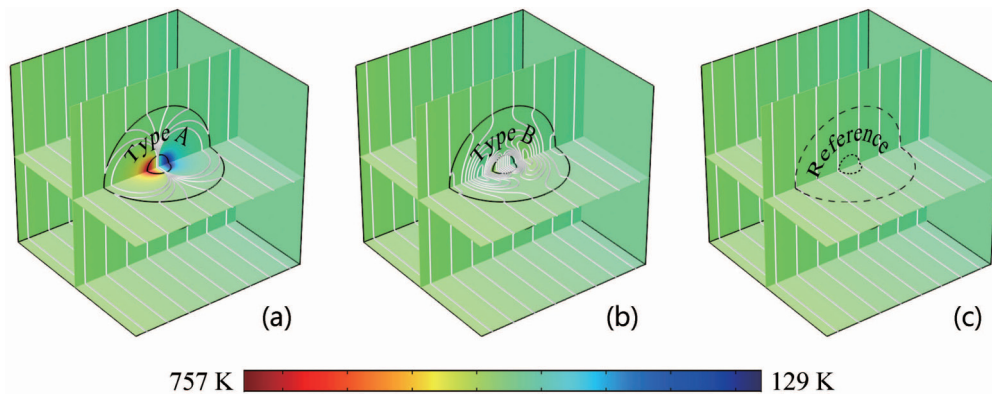


FIG. 6. Finite-element simulations of three-dimensional golden touch for (a) type A, (b) type B, and (c) reference. Concrete parameters: (a–c) simulation box is $20 \times 20 \times 20$ cm, $r_s = 6.4$ cm, $r_c = 1.28$ cm, $\kappa_c = \kappa_m = 5 \text{ Wm}^{-1}\text{K}^{-1}$, (a) $\kappa_s = -2.501 \text{ Wm}^{-1}\text{K}^{-1}$, (b) $\kappa_s = \text{diag}(-10, 77.455, 77.455) \text{ Wm}^{-1}\text{K}^{-1}$, and (c) $\kappa_s = 5 \text{ Wm}^{-1}\text{K}^{-1}$. The left and right boundaries are, respectively, set at 463 K and 423 K, and other boundaries are insulated.

temperature gradient between the matrix in Figs. 5(a)–5(c) and Fig. 5(d) validates the theoretically predicted golden touch.

The results of three-dimensional golden touch are presented in Fig. 6. We set the core fraction as 0.008. Type A and type B golden touch are, respectively, designed according to Eqs. (13) and (14). It is found that the external temperature distribution in Figs. 6(a)–6(c) is totally the same, which again validates the golden touch.

V. DISCUSSION AND CONCLUSION

When discussing golden touch, a puzzling phenomenon is that type C golden touch cannot be extended from two to three dimensions. In other words, type C golden touch is a unique phenomenon which exists in only two dimensions. In fact, low-dimensional heat transfer at a microscopic scale has been found to have many unique properties, such as the nonconvergence effect and size effect of the thermal conductivity [23]. However, the uniqueness of low-dimensional heat transfer has never been discovered at a macroscopic scale, such as thermal metamaterials including but not limited to thermal cloaks [5–10], thermal concentrators [6,11–14], and thermal camouflage [15–21]. Therefore, type C golden touch might open a gate to explore unique properties in low-dimensional heat transfer at a macroscopic scale.

Moreover, type C golden touch in the first quadrant also seems to be distinct, for it is the only golden touch which requires no apparent negative thermal conductivity; see Figs. 2(b) and 2(d). Although apparent negative thermal conductivity does not exist in nature, it can be realized by active materials containing heat sources [24–26]. We take two-dimensional type A golden touch [Fig. 5(a)] as an example. We set the thermal conductivity of the shell with a positive value which is different from that of the core. To realize the same effect of golden touch, we add continuous sources [Fig. 7(a)] and discontinuous sources [Fig. 7(b)] on the boundaries of the shell. The same temperature profile between Figs. 7(a) and 7(b) and Fig. 5(a) validates that the scheme of adding sources works indeed. For experimental realization, Ref. [27] demonstrates a device to realize the discontinuous sources, which makes apparent negative thermal conductivities feasible for experiments.

We also first derive the effective thermal conductivity under the demarcation point, i.e., $\kappa_{\theta\theta}/\kappa_{rr} < 0$ for two dimensions [Eq. (2)] and $\kappa_{\theta\theta}/\kappa_{rr} < -1/8$ for three dimensions [Eq. (10)]. This helps to reveal the quasiperiodic variation with core fraction; see Figs. 3(d)–3(f) and Figs. 4(d)–4(f), which is dramatically different from the well-known effective medium theories like the Maxwell-Garnett formula [28] and the Bruggeman formula [29]. This may further provide guidance for exploring nonlinear effects [30] beyond the framework of the Maxwell-Garnett formula or Bruggeman formula. Moreover, one reliable approach to realize these special thermal conductivities is to design multilayer structures with effective medium theory. In this way, the complex parameters can be obtained with several homogeneous and isotropic materials which are easy to get.

In summary, golden touch proposed in this work can extend the core property to shell with extremely small

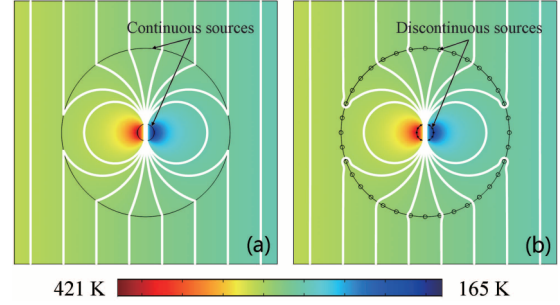


FIG. 7. Realization of apparent negative thermal conductivity by adding (a) continuous sources and (b) discontinuous sources. The parameters are the same as those in Fig. 5(a), except for the shell which is set as $\kappa_s = 1 \text{ Wm}^{-1}\text{K}^{-1}$. (a) Continuous sources are applied on the inner and outer boundaries of the designed shell, which obey the continuous temperature distribution $T = -81.92x/r_{c,s}^2 + 293$, where $r_c = 0.64 \text{ cm}$ ($r_s = 6.4 \text{ cm}$) is the inner (or outer) radius of the designed shell. x represents abscissa whose origin locates in the center of the simulation box. For the inner boundary, x ranges from $-r_c$ to r_c which makes the temperature T range from 421 K to 165 K; for the outer boundary, x ranges from $-r_s$ to r_s which makes temperature T range from 306 K to 280 K. (b) Twelve discontinuous sources (with radius 0.05 cm) and 36 discontinuous sources (with radius 0.15 cm) are, respectively, applied on the inner and outer boundaries. The discontinuous temperatures are calculated from the continuous temperature distribution in (a) according to the source abscissas.

core fraction, which has potential applications in thermal camouflage, thermal management, etc. Furthermore, golden touch can be directly extended to electrostatics and magnetostatics where permittivity and permeability play the same role as thermal conductivity in thermotics. Golden touch in magnetostatics may also offer guidance for magnetostatic camouflage [31–33].

ACKNOWLEDGMENTS

We acknowledge the financial support by the National Natural Science Foundation of China under Grant No. 11725521, and by the Science and Technology Commission of Shanghai Municipality under Grant No. 16ZR1445100.

APPENDIX

The dominant equation of heat conduction is

$$\nabla \cdot (-\kappa \nabla T) = 0, \quad (\text{A1})$$

where κ and T are, respectively, tensorial thermal conductivity and temperature.

We firstly discuss the two-dimensional core-shell structure and put it into an infinite matrix with thermal conductivity κ_m . Equation (A1) can be expanded in cylindrical coordinates as

$$\frac{\partial}{\partial r} \left(r \kappa_{rr} \frac{\partial T}{\partial r} \right) + \frac{\partial}{\partial \theta} \left(\kappa_{\theta\theta} \frac{\partial T}{r \partial \theta} \right) = 0. \quad (\text{A2})$$

The general solution of Eq. (A2) is

$$T(\kappa_{\theta\theta}/\kappa_{rr} > 0) = A_0 + B_0 \ln r + \sum_{i=1}^{\infty} [A_i \sin(i\theta) + B_i \cos(i\theta)] r^{im_1} + \sum_{i=1}^{\infty} [C_i \sin(i\theta) + D_i \cos(i\theta)] r^{im_2}, \quad (\text{A3})$$

$$T(\kappa_{\theta\theta}/\kappa_{rr} < 0) = E_0 + F_0 \ln r + \sum_{i=1}^{\infty} [E_i \sin(i\theta) + F_i \cos(i\theta)] \sin(in \ln r) + \sum_{i=1}^{\infty} [G_i \sin(i\theta) + H_i \cos(i\theta)] \cos(in \ln r), \quad (\text{A4})$$

where $m_{1,2} = \pm \sqrt{\kappa_{\theta\theta}/\kappa_{rr}}$, and $n = \sqrt{-\kappa_{\theta\theta}/\kappa_{rr}}$. Here $\kappa_{\theta\theta}/\kappa_{rr} = 0$ is the demarcation point.

The temperature distribution of the core (T_c), shell (T_s), and matrix (T_m) can then be determined by the following boundary conditions:

$$\begin{cases} T_c < \infty, \\ T_c(r_c) = T_s(r_c), \\ T_s(r_s) = T_m(r_s), \\ (-\kappa_c \partial T_c / \partial r)_{r_c} = (-\kappa_{rr} \partial T_s / \partial r)_{r_c}, \\ (-\kappa_{rr} \partial T_s / \partial r)_{r_s} = (-\kappa_m \partial T_m / \partial r)_{r_s}, \\ \nabla T_m(r \rightarrow \infty) = \nabla T_0, \end{cases} \quad (\text{A5})$$

where ∇T_0 represents the external uniform thermal field gradient.

For the symmetric core-shell structure and boundary conditions, we require only keeping several terms of $i = 1$ in Eqs. (A3) and (A4):

$$T(\kappa_{\theta\theta}/\kappa_{rr} > 0) = A_0 + B_1 r^{m_1} \cos \theta + D_1 r^{m_2} \cos \theta, \quad (\text{A6})$$

$$T(\kappa_{\theta\theta}/\kappa_{rr} < 0) = E_0 + F_1 \cos \theta \sin(n \ln r) + H_1 \cos \theta \cos(n \ln r). \quad (\text{A7})$$

Therefore, for an isotropic matrix, we can obtain $T_m = A_0 + B_1 r \cos \theta + D_1 r^{-1} \cos \theta$. We set D_1 as zero to ensure the external thermal field undistorted. Then we can derive the effective thermal conductivity of the core-shell structure κ_e as Eqs. (1) and (2).

We next discuss the three-dimensional core-shell structure and put it into an infinite matrix with thermal conductivity κ_m . Equation (A1) can be expanded in spherical coordinates as

$$\frac{1}{r} \frac{\partial}{\partial r} \left(r^2 \kappa_{rr} \frac{\partial T}{\partial r} \right) + \frac{1}{\sin \theta} \frac{\partial}{\partial \theta} \left(\sin \theta \kappa_{\theta\theta} \frac{\partial T}{r \partial \theta} \right) = 0. \quad (\text{A8})$$

The general solution of Eq. (A8) is

$$T(\kappa_{\theta\theta}/\kappa_{rr} \geq 0) = A_0 + B_0 r^{-1} + \sum_{i=1}^{\infty} (A_i r^{s_1} + B_i r^{s_2}) P_i(\cos \theta), \quad (\text{A9})$$

$$T(0 > \kappa_{\theta\theta}/\kappa_{rr} > -1/8) = C_0 + D_0 r^{-1} + \sum_{i=1}^j (C_i r^{s_1} + D_i r^{s_2}) P_i(\cos \theta) + \sum_{i=j+1}^{\infty} r^{-1/2} [E_i \sin(t \ln r) + F_i \cos(t \ln r)] P_i(\cos \theta), \quad (\text{A10})$$

$$T(\kappa_{\theta\theta}/\kappa_{rr} < -1/8) = G_0 + H_0 r^{-1} + \sum_{i=1}^{\infty} r^{-1/2} [G_i \sin(t \ln r) + H_i \cos(t \ln r)] P_i(\cos \theta), \quad (\text{A11})$$

where $s_{1,2} = [-1 \pm \sqrt{1 + 4i(i+1)\kappa_{\theta\theta}/\kappa_{rr}}]/2$, $t = \sqrt{-1 - 4i(i+1)\kappa_{\theta\theta}/\kappa_{rr}}/2$, and $j = \text{INT}[(-1 + \sqrt{1 - \kappa_{rr}/\kappa_{\theta\theta}})/2]$, where i is the summation index in Eqs. (A9)–(A11), and $\text{INT}[\dots]$ is the integral function with respect to \dots . P_i is Legendre polynomials.

We find that Eqs. (A9) and (A10) are essentially the same with similar boundary conditions of Eq. (A5), for we require only keeping several terms of $i = 1$:

$$T(\kappa_{\theta\theta}/\kappa_{rr} > -1/8) = A_0 + (A_1 r^{s_1} + B_1 r^{s_2}) \cos \theta, \quad (\text{A12})$$

$$T(\kappa_{\theta\theta}/\kappa_{rr} < -1/8) = G_0 + r^{-1/2} [G_1 \sin(t \ln r) + H_1 \cos(t \ln r)] \cos \theta. \quad (\text{A13})$$

Therefore, $\kappa_{\theta\theta}/\kappa_{rr} = -1/8$ is the real demarcation point. For isotropic matrix, we can obtain $T_m = A_0 + (A_1 r + B_1 r^{-2}) \cos \theta$. We set B_1 as zero to ensure the external thermal field undistorted. Then we can derive the effective thermal conductivity of the core-shell structure κ_e as Eqs. (9) and (10).

- [1] D. J. Bergman and D. Stroud, Physical properties of macroscopically inhomogeneous media, *Solid State Phys.* **46**, 147 (1992).
- [2] J. P. Huang and K. W. Yu, Enhanced nonlinear optical responses of materials: Composite effects, *Phys. Rep.* **431**, 87 (2006).
- [3] S. Yang, L. J. Xu, R. Z. Wang, and J. P. Huang, Full control of heat transfer in single-particle structural materials, *Appl. Phys. Lett.* **111**, 121908 (2017).
- [4] L. J. Xu, C. R. Jiang, J. Shang, R. Z. Wang, and J. P. Huang, Periodic composites: Quasi-uniform heat conduction, Janus thermal illusion, and illusion thermal diodes, *Eur. Phys. J. B* **90**, 221 (2017).
- [5] C. Z. Fan, Y. Gao, and J. P. Huang, Shaped graded materials with an apparent negative thermal conductivity, *Appl. Phys. Lett.* **92**, 251907 (2008).
- [6] S. Narayana and Y. Sato, Heat Flux Manipulation with Engineered Thermal Materials, *Phys. Rev. Lett.* **108**, 214303 (2012).
- [7] T. C. Han, T. Yuan, B. W. Li, and C. W. Qiu, Homogeneous thermal cloak with constant conductivity and tunable heat localization, *Sci. Rep.* **3**, 1593 (2013).
- [8] H. Y. Xu, X. H. Shi, F. Gao, H. D. Sun, and B. L. Zhang, Ultrathin Three-Dimensional Thermal Cloak, *Phys. Rev. Lett.* **112**, 054301 (2014).
- [9] T. C. Han, X. Bai, D. L. Gao, J. T. L. Thong, B. W. Li, and C. W. Qiu, Experimental Demonstration of a Bilayer Thermal Cloak, *Phys. Rev. Lett.* **112**, 054302 (2014).
- [10] Y. G. Ma, Y. C. Liu, M. Raza, Y. D. Wang, and S. L. He, Experimental Demonstration of a Multiphysics Cloak: Manipulating Heat Flux and Electric Current Simultaneously, *Phys. Rev. Lett.* **113**, 205501 (2014).
- [11] T. C. Han, J. J. Zhao, T. Yuan, D. Y. Lei, B. W. Li, and C. W. Qiu, Theoretical realization of an ultra-efficient thermal energy harvesting cell made of natural materials, *Energ. Environ. Sci.* **6**, 3537 (2013).
- [12] M. Moccia, G. Castaldi, S. Savo, Y. Sato, and V. Galdi, Independent Manipulation of Heat and Electrical Current Via Bifunctional Metamaterials, *Phys. Rev. X* **4**, 021025 (2014).
- [13] T. Y. Chen, C. N. Weng, and Y. L. Tsai, Materials with constant anisotropic conductivity as a thermal cloak or concentrator, *J. Appl. Phys.* **117**, 054904 (2015).
- [14] X. Y. Shen, Y. Li, C. R. Jiang, Y. S. Ni, and J. P. Huang, Thermal cloak-concentrator, *Appl. Phys. Lett.* **109**, 031907 (2016).
- [15] T. C. Han, X. Bai, J. T. L. Thong, B. W. Li, and C. W. Qiu, Full control and manipulation of heat signatures: Cloaking, camouflage and thermal metamaterials, *Adv. Mater.* **26**, 1731 (2014).
- [16] T. Z. Yang, X. Bai, D. L. Gao, L. Z. Wu, B. W. Li, J. T. L. Thong, and C. W. Qiu, Invisible sensors: Simultaneous sensing and camouflaging in multiphysical fields, *Adv. Mater.* **27**, 7752 (2015).
- [17] T. Z. Yang, Y. Su, W. Xu, and X. D. Yang, Transient thermal camouflage and heat signature control, *Appl. Phys. Lett.* **109**, 121905 (2016).
- [18] L. J. Xu, R. Z. Wang, and J. P. Huang, Camouflage thermotics: A cavity without disturbing heat signatures outside, *J. Appl. Phys.* **123**, 245111 (2018).
- [19] L. J. Xu and J. P. Huang, A transformation theory for camouflaging arbitrary heat sources, *Phys. Lett. A* **382**, 3313 (2018).
- [20] R. Hu, S. L. Zhou, Y. Li, D. Y. Lei, X. B. Luo, and C. W. Qiu, Illusion thermotics, *Adv. Mater.* **30**, 1707237 (2018).
- [21] S. L. Zhou, R. Hu, and X. B. Luo, Thermal illusion with twinborn-like heat signatures, *Int. J. Heat Mass Transf.* **127**, 607 (2018).
- [22] <http://www.comsol.com>
- [23] S. Lepri, R. Livi, and A. Politi, Thermal conduction in classical low-dimensional lattices, *Phys. Rep.* **377**, 1 (2003).
- [24] M. Wegener, Metamaterials beyond optics, *Science* **342**, 939 (2013).
- [25] Y. Gao and J. P. Huang, Unconventional thermal cloak hiding an object outside the cloak, *Europhys. Lett.* **104**, 44001 (2013).
- [26] X. Y. Shen and J. P. Huang, Thermally hiding an object inside a cloak with feeling, *Int. J. Heat Mass Transf.* **78**, 1 (2014).
- [27] D. M. Nguyen, H. Y. Xu, Y. M. Zhang, and B. L. Zhang, Active thermal cloak, *Appl. Phys. Lett.* **107**, 121901 (2015).
- [28] J. C. Maxwell-Garnett, Colours in metal glasses and in metallic films, *Philos. Trans. R. Soc. London Ser. A* **203**, 385 (1904).
- [29] D. A. G. Bruggeman, Calculation of various physics constants in heterogenous substances: Dielectricity constants and conductivity of mixed bodies from isotropic substances, *Ann. Phys. Leipzig* **24**, 636 (1935).
- [30] G. L. Dai, J. Shang, R. Z. Wang, and J. P. Huang, Nonlinear thermotics: Nonlinearity enhancement and harmonic generation in thermal metasurfaces, *Eur. Phys. J. B* **91**, 59 (2018).
- [31] F. Gomory, M. Solovyov, J. Souc, C. Navau, J. P. Camps, and A. Sanchez, Experimental realization of a magnetic cloak, *Science* **335**, 1466 (2012).
- [32] R. M. Batlle, A. Parra, S. Laut, N. D. Valle, C. Navau, and A. Sanchez, Magnetic Illusion: Transforming a Magnetic Object into Another Object by Negative Permeability, *Phys. Rev. Appl.* **9**, 034007 (2018).
- [33] W. Jiang, Y. G. Ma, and S. L. He, Static Magnetic Cloak without a Superconductor, *Phys. Rev. Appl.* **9**, 054041 (2018).